EFFECTS OF ADVANCED SEISMIC ANALYSIS WITH ARMA MODELS: ASSESSING DAMAGE IMPACT AND HYSTERESIS IN EARTHQUAKE TIME SERIES

Abderrazek MENASRI[1*] , Ahmed SEDDIKI[1] , Tahar BRAHIMI[2],
Abdelmadjid BOUBAYA[3]

[1] *Civil Engineering Department, Technology Faculty, M'sila University, Algeria*
[2] *Laghouat Normal School (ENSL), Algeria*
[3] *Research Laboratory in Civil Engineering, Biskra University, Algeria*
*corresponding author, *abderrazek.menasri@univ-msila.dz*

Actual records of strong motion acceleration cannot meet engineering requirements. The simulated seismic waves become an equivalent source of seismic wave input. The time-varying autoregressive moving average (ARMA) process is a straightforward and effective method for simulating seismic ground motions. This model can accurately replicate the non-stationary amplitude and frequency characteristics of seismic ground accelerations, making it useful for assessing damage indicators, which are then compared to spectra derived from real seismic records. It is demonstrated that the chosen ARMA(2,1) model and the applied algorithm effectively capture the characteristics of real seismic records, even with the varying frequency content.

Keywords: seismic waves; non-stationary; damage predictors; ARMA model.

1. Introduction

Acceleration data presented as time series are a subject of considerable interest and significance in various applications. These time series exhibit significant irregularities in both amplitude and frequency characteristics, which are subject to change over time. Essentially, all acceleration data can be viewed as time series with nonstationary characteristics, and each acceleration time series is essentially a single realization of a nonstationary stochastic process (Sakellariou & Fassois, 2006; Zheng & Mita, 2007). To model these time series effectively, two main approaches are employed: in the frequency and in the time domains. The time-varying nature of the frequency content is taken into account by utilizing an evolutionary density function, a valuable tool for characterizing the frequency content in these data (Carden & Brownjohn, 2008). The connection between theoretical concepts and practical applications has led to the development of a practical technique for modeling acceleration using ARMA models (Ay & Wang, 2014; Luo & Yu, 2017). These models offer the flexibility needed to accurately represent real acceleration time series data (Bodeux & Golinval, 2001).

Analysis of linear and nonlinear response spectra reveals that the ARMA(2,1) process, when applied to simulated acceleration time series, effectively captures the key characteristics of acceleration records (Johnson *et al.*, 2004; El-Choum, 2014). This approach also characterizes dependency patterns in displacement plasticity and hysteretic energy (Nair *et al.*, 2006; Zhang, 2007). By analyzing response spectra from ARMA models, dynamic structural responses are assessed with precision, an approach also used in nonlinear analysis of concrete dams (Ouzandja *et al.*, 2023). In our study, the ARMA(2,1) model, analyzed in detail by Box *et al.* (2015), was found most suitable for computing hysteretic energy.

2. Earthquake process model modelling

2.1. Acceleration time series process models (ARMA)

ARMA (p, q) process model can be represented as follows:

$$z_t - \varphi_1 z_{t-1} - ... - \varphi_p z_{t-p} = a_t - \theta_1 a_{t-1} - ... - \theta_q a_{t-q}, \tag{2.1}$$

where φ_i and φ_j are constant coefficients; (p, q) is the order of the model.

The model contains $p + q + 1$ unknown parameters, which are usually estimated from data based on maximum likelihood and the model order is based on the Akaike information criteria.

2.2. Autocorrelation functions

To determine the appropriate order (p, q) for the ARMA model, representing an acceleration time series, it is essential to examine the theoretical autocorrelation function, $R(k)$. The theoretical autocovariance function, $C(k)$, can be derived by multiplying Eq. (2.1) by z_t and taking expectations (Brahimi, 1989):

$$C(k) = \varphi_1 C(k-1) + ... + \varphi_p C(k-p) + C_{za}(k) - \theta_1 C_{za}(k-1) - ... - \theta_q C_{za}(k-q), \tag{2.2}$$

where

$$C_{za}(k) = E[z_{t-k} \cdot a_t]. \tag{2.3}$$

The autocorrelation function $R(k)$ is obtained by dividing Eq. (2.2) by $C(0)$ and a similar form is obtained:

$$R(k) = \varphi_1 R(k-1) + ... + \varphi_p R(k-p) + RC_{za}(k) - \theta_1 R_{za}(k-1) - ... - \theta_q R_{za}(k-q). \tag{2.4}$$

The fact that the values of z_{t-k} are correlated only to white noise values up to time $t - k$ implies that:

$$C_{za}(k) = 0 \qquad \text{for} \quad k > 0. \tag{2.5}$$

Thus, for processes using AR, the function takes the form of an exponential decay or series of waves as the lag k increases. Alternatively, for MA, when the lag k reaches a specific order g, the function becomes equal to zero. Finally, when the ARMA process is used, when the first $g - p$ lag is overcome, the function takes the form of a combination of exponential decay waves.

2.3. The function of partial autocorrelation

The partial autocorrelation function describes the time dependence of the series, when combined with the use of AR, it becomes possible to accurately identify the order and type of the model being estimated. For stationary autoregressive (AR) processes, the autocorrelation function continues indefinitely.

Therefore, characterizing the autoregressive process involves counting the non-zero autocorrelation terms. The theoretical partial autocorrelation function $P(k)$ is calculated using the Yule–Walker equations. For a stationary and invertible ARMA process, the partial autocorrelation function $P(k)$ decays with a damped exponential or sine wave pattern, influenced by moving average parameters after the first $p - q$ lags (Brahimi, 1989).

2.4. AIC criteria

One major challenge in this study was estimating both the number and values of model parameters to minimize the discrepancy between the simulated model and the actual time series. The model order was determined using the Akaike information criterion (AIC), while the parameters were estimated through a nonlinear least squares approach. AIC focuses on maximum information criteria, considering entropy and Kullback–Liebler information for independent observations. For stationary time series, the optimal model minimizes this criterion:

$$\text{AIC}(p,q) = N \ln(\sigma_a^2) + 2(p+q), \tag{2.6}$$

where N is the sample size, and σ_a^2 is the maximum likelihood estimate of the residual variance.

In this analysis, the ARMA(1,1), ARMA(1,2), ARMA(2,1), and ARMA(2,2) models were used for each seismic event. The final model selection for each earthquake was made based on a comparative AIC evaluation across the proposed models.

2.5. Modulating function

Another challenge in the simulation was estimating the variance or the envelope function. Variance regulates the non-stationarity of the process and considers statistical parameters, including structural responses or extreme acceleration values. The variance for the acceleration time series data, z_t, considered as random variables, is expressed as

$$\sigma_a^2 = E(z_t - \mu_t). \tag{2.7}$$

The common assumption $E(z_t) = 0$ is used in acceleration time series simulations, employing equally weighted two-second windows with 0.02-second intervals, estimating variance as

$$f_Z^2(t) = \frac{1}{100} \sum_{T-50}^{t+50} z_T^2. \tag{2.8}$$

Here, $f(t)$ approximates the modulating function, although it lacks criteria to differentiate between stationary and non-stationary data. Practically, a variance function with few parameters is ideal (Brahimi, 1989). This study uses a moving window with 0.5-second intervals to determine the variance across three acceleration time series, with MATLAB performing all necessary calculations.

2.6. Parametric envelope function

To simplify practical applications, a variance function with limited parameters is desirable. A smoothed function with limited parameters is used here (Brahimi, 1989):

$$s(t) = \alpha \exp\left(-\frac{t-\beta}{\gamma}\right)^2, \tag{2.9}$$

where α, β, γ are constants found by fitting the function to the estimated variance using the least squares method. This function is effective in fitting modulating functions with narrow peaks.

3. Procedure for modeling

To model ground motion acceleration as the ARMA process, the data is first transformed for stationarity by isolating the period of significant shaking. The ARMA modeling follows this procedure (Menasri *et al.*, 2012):

– calculate the experimental modulating function and normalize the data;
– assume an analytical form for $s(t)$ and estimate its parameters;

– calculate autocorrelation functions;
– choose model order (p, q) based on autocorrelation;
– estimate model coefficients using maximum likelihood, applying the Kalman filter for time-varying coefficients;
– select the model with the lowest AIC.

The three recorded accelerograms framed below were selected for our case.

Table 1. Characteristics of real earthquakes (Menasri, 2012).

Event	Affroun EW	Affroun NS	Affroun V
Magnitude	6.8	6.8	6.8
Duration [s]	80	80	80
Acceleration max × g	0.1644	0.09	0.03
Number of points	16001	16001	16001

4. Application of ARMA models

4.1. Models adopted

For this study, the ARMA model with a parametric envelope function was chosen to simplify parameter estimation for design purposes. Modeling begins with a modulating function to stabilize the series, which is then fitted to a smoothed parametric envelope function (e.g., Eq. (2.9)) effective for narrow peaks (Brahimi, 1989). Parameters are estimated from the stabilized series.

4.2. Acceleration time series

Three acceleration time series, including Affroun with 16000 data points (0.005 second digitization increment), were consistently used. The main difference between the series was the number of data points required for estimation, with the plots shown in Fig. 1.
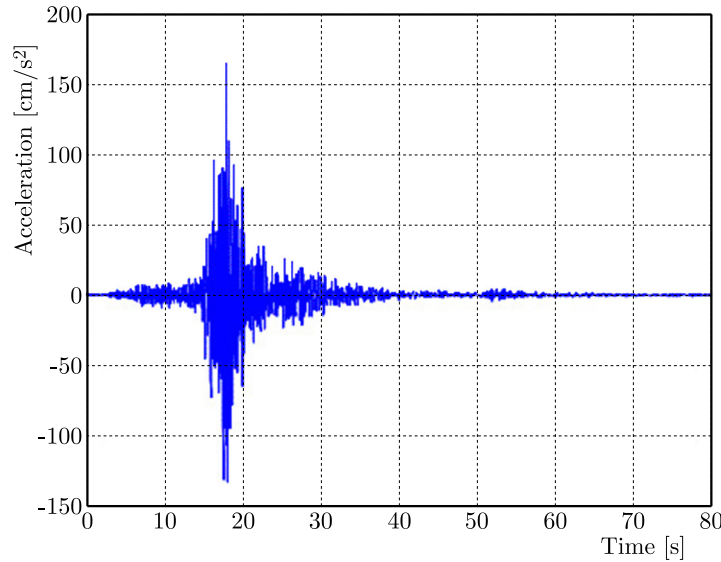

Fig. 1. Time series of acceleration measurements at the Affroun station in the East-West direction.

As the first step in model identification, the modulating function $f(t)$ was computed for each measured acceleration record using Eq. (2.2).

Figure 2 shows the appearance and envelope functions for Affroun EW, NS, and V earthquakes. It is evident that non-stationarity is significant across events.
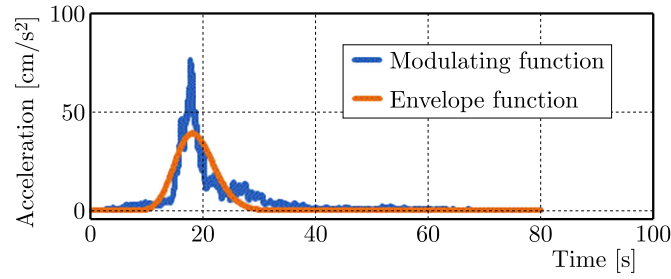
Fig. 2. Modulating and envelope functions extracted from the Affroun East-West acceleration data.

The single-peak envelope function in Eq. (2.9) is fitted to each measured modulating function using the least squares method, with results shown for four acceleration series in Fig. 2.

The original acceleration record and the obtained modulating function allow the estimation of the stabilized acceleration series, as shown for the El Affroun EW event in Fig. 3. The resulting series has an approximate variance of one and a mean near zero, with the frequency content incorporated into ARMA model parameters.
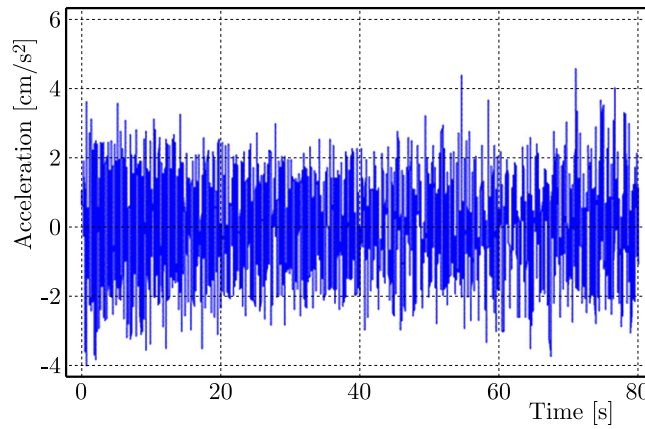

Fig. 3. Stabilized acceleration time series for the Affroun East-West component.

5. Results

Estimated autocorrelations for the three stabilized time series from measured records are shown in Fig. 4. The rapid decay of autocorrelations indicates that no roots of the characteristic equation are near the unit circle boundary, confirming stationarity.
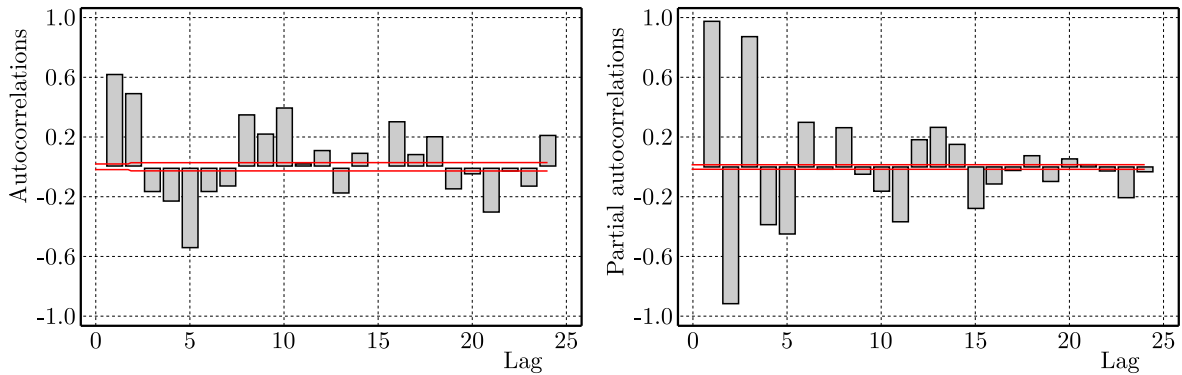

Fig. 4. Estimated and partial autocorrelation functions for the Affroun East-West acceleration data.

Partial autocorrelation functions are estimated for each record by fitting successive autoregressive processes of the order k in MATLAB, with results for Affroun EW in Fig. 4.

The partial autocorrelation function for the Affroun series indicates that after the lag $q = 2$ or $q = 3$, correlations decline, suggesting an ARMA model order with $p - q = 2$ or 3. Models based on AR and partial AR functions were tested for three events, using maximum likelihood estimates approximated by the least squares method. The model order selection was guided by the AIC criteria, and ARMA simulations with one or two MA terms were found optimal. Table 2 presents AIC values for ARMA models, showing ARMA(2,1) as the best fit for Affroun series.

Table 2. Application of AIC criteria to different ARMA models (Menasri, 2012).

Model	AIC (Affroun EW)	AIC (Affroun NS)	AIC (Affroun V)
ARMA(1,1)	-4.21635	-4.21958	-3.64068
ARMA(1,2)	-5.11995	-5.29379	-4.78432
ARMA(2,1)	-5.84522^*	-5.73424^*	-5.09023
ARMA(2,2)	-5.71991	-5.61231	-5.26325^*

*Optimal set by AIC criterion. [Source: Menasri (2012)].

Table 3 lists the AR parameters φ_1, φ_2, the moving average θ_1, θ_2, while Table 4 provides envelope function parameters α, β, γ, with 95 % confidence limits. Stability and invisibility conditions are verified by the coefficients.

Table 3. Parameters of the selected models (Menasri, 2012).

Parameters	Affroun EW	Affroun NS	Affroun V
AR (1)	1.82986	1.85144	1.80244
AR (2)	-0.879019	-0.900216	-0.888599
MA (1)	-0.7313	-0.634745	-0.754022
σ_a	0.0543099	0.0571895	0.0785381

Table 4. Parameters of the envelope function.

Event	Parameters envelope function		
	α	β	γ
Affroun EW	3.475e-8	10.78	0.59
Affroun NS	8.48e-8	9.958	0.5285
Affroun V	9.61e-9	10.91	0.6055

6. Acceleration time series

Simulated ARMA process systems, using a time-based approach, yield good results with a limited number of parameters. The method involved generating stationary time series via the ARMA model, then applying the envelope function. The ARMA model was treated as a linear combination of Gaussian random variables (a_t) and existing values (z_t), enabling recursive simulation of the time series. A simulation of the acceleration time series shown in Fig. 5.

The comparison of the main characteristics of real and simulated earthquakes is shown in Table 5.

The results show that the ARMA(2,1) process, combined with the envelope function parameters, better represents the Affroun EW, NS, and V events.
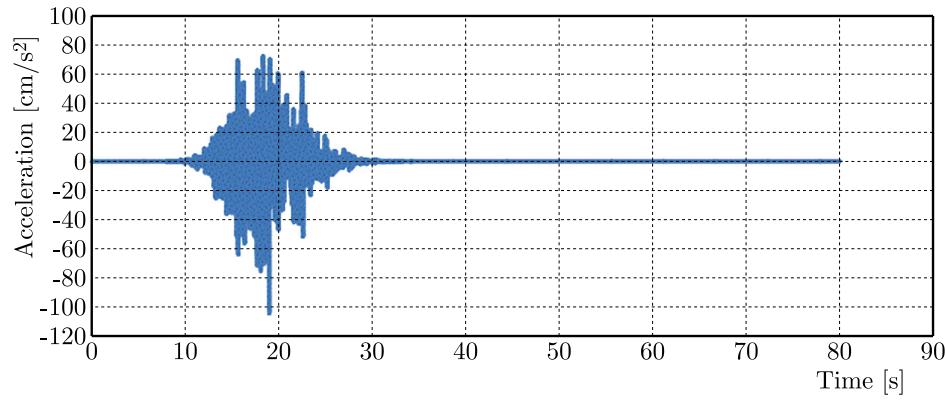
Fig. 5. Simulated acceleration time series for the Affroun East-West component.

Table 5. Characteristics of real and simulated earthquakes.

Earthquake		Affroun EW	Affroun NS	Affroun V
Real	Maximum acceleration × g	0.1644	0.09	0.03
Simulated	Maximum acceleration × g	0.115	0.08	0.022
	Duration [s]	80	80	80

7. Response spectra

7.1. Measures of damage

Various methods have been developed to assess the impact of earthquakes on both linear and non-linear structures, with significant contributions from researchers such as Lin, Mahin, and Grigorio. The pursuit of precision plays a pivotal role in structural analysis, making the utilization of highly sensitive predictive models a matter of significant importance. More specifically, ARMA models are recognized as effective analytical tools for both qualitatively and quantitatively describing the non-stationary nature of input data in structural analysis. Consequently, each acceleration time series under examination is regarded as an outcome arising from a sequence of multiple stochastic processes.

As a result, each acceleration time series being analyzed is considered the outcome of a series of multiple stochastic processes.

Simultaneously, the characterization of ground acceleration time series can be achieved through structural response spectra where a measure of the response damage is graphically represented, where a measure of response damage is plotted as a function of time period.

Single degree of freedom and viscous damping systems are used to calculate these spectra as shown schematically in Fig. 6. It is worth noting that these systems can exhibit either bilinear or degenerate stiffness. This implies that for successful modeling, an integration method must
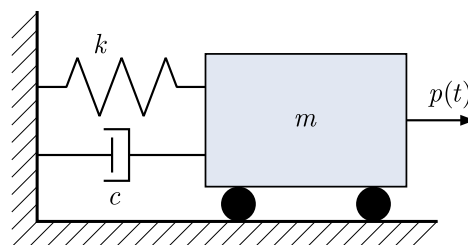

Fig. 6. One-degree-of-freedom system.

be employed that takes linear acceleration into account at each computational step. This approach enables the derivation of spectral responses for the series, as represented by the equation:

$$M\ddot{U}(t) + c\dot{U}(t) + R(u,t) = -M\ddot{U}_g(t), \tag{7.1}$$

where M is the mass, u is the relative displacement of mass, c is the damping coefficient, $\ddot{U}_g$ is the ground acceleration, R is the restoring force.

7.2. Peak displacement ductility

For design, it suffices to consider the maximum response value:

$$U_{\max} = |U_{\max}(t)|, \tag{7.2}$$

where $U_{\max}(t)$ represents the maximum displacement during an earthquake, and $U_{\max}$ denotes ultimate deformation capacity under monotonic loading.

Responses $U_{\max}(t)$ are obtained by assuming a linear acceleration at each time step, we make a numerical integration of the general equation.

This function enables us to relate the system's maximum value to its natural oscillation period, facilitating the creation of a spectrum for systems where damping values and the periodic range are the same.

7.3. Hysteretic energy in a normalized form

The hysteretic energy is derived by dividing the dissipation energy by twice the absorbed energy. For structures with hysteretic load-deformation, the dissipation energy is:

$$E_h(t) = \int_0^t R(u,t)\dot{u}(t)\,\mathrm{d}t - E_s(t), \tag{7.3}$$

where $E_s(t)$ is elastic deformation energy:

$$E_s = \frac{1}{2}K_y U_y^2, \tag{7.4}$$

where K_y the stiffness after elasticity, U_y is the initial elastic displacement.

The bilinear model, often used in this context, is defined by three primary parameters: U_y the initial yield displacement; K_1 the initial elastic stiffness; and K_y the post-yielding stiffness. As displacement increases, this model provides the corresponding restoring force:

$$R(u,t) = \begin{cases} R(u,t) = K_1 u(t) & \text{if } U_y \geq u(t), \\ R(u,t) = K_y(u(t) - u_z) & \text{if } U_y < u(t). \end{cases} \tag{7.5}$$

The value u_z represents at the yield envelope intersects the displacement axis. During unloading, stiffness remains at the initial level until the yield envelope is reached.

The normalized hysteric energy is given as follows:

$$E_{NH} = 1 + \frac{E_H}{R_y U_y}, \tag{7.6}$$

where $R_y = K_y U_y$ represents the force at yield, E_H the hysteretic energy resulting from inelastic deformation.

7.4. Application and numerical results

Several ARMA models proved highly suitable for analyzing three distinct time series with varying data points. For the response analysis, damping coefficients (ε) were set to 0.05, and the yield coefficient (Y) was calculated as $Y = R_y/Mg$, ranging from 0.05 to 0.3. The hysteretic energy was computed using alternative output coefficients, and mean displacement ductility was used to establish demand spectra for the hysteretic energy (Brahimi, 2021). Confidence intervals were estimated using standard deviations, and spectral values decreased as the period increased.
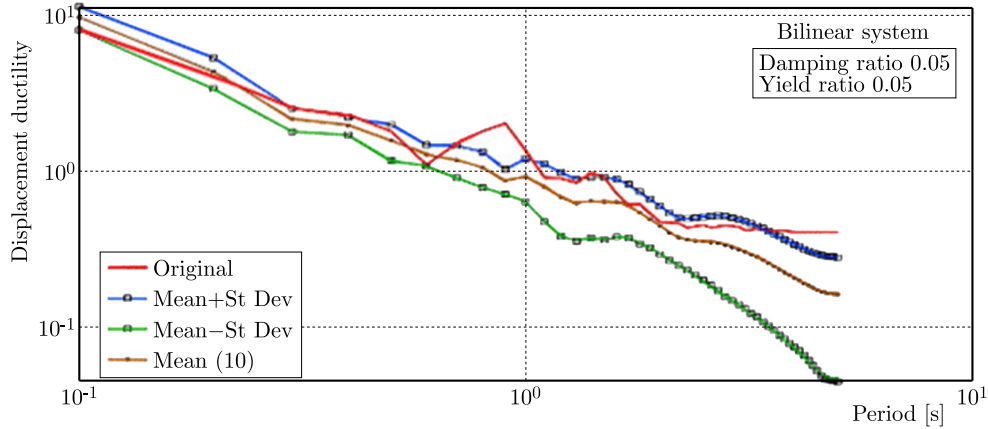

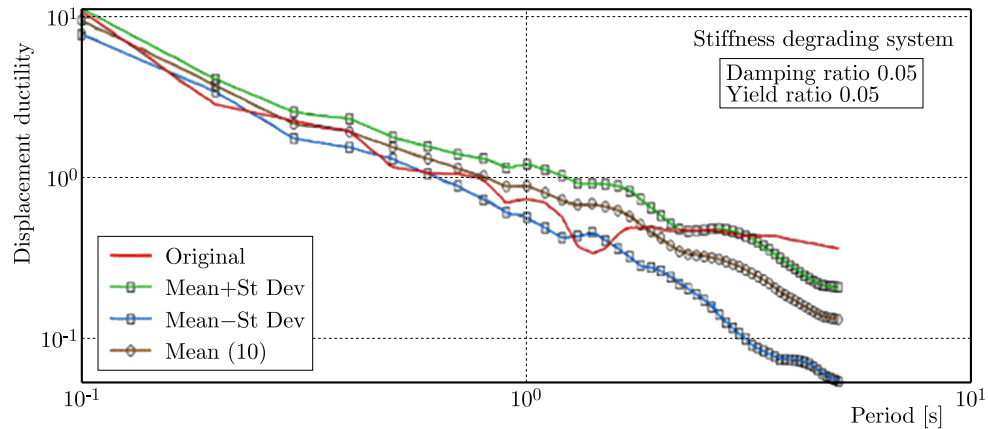Fig. 7. Displacement ductility in a bilinear system as a function of period for a given damping ratio.

Fig. 8. System for modeling stiffness degradation with respect to displacement ductility.
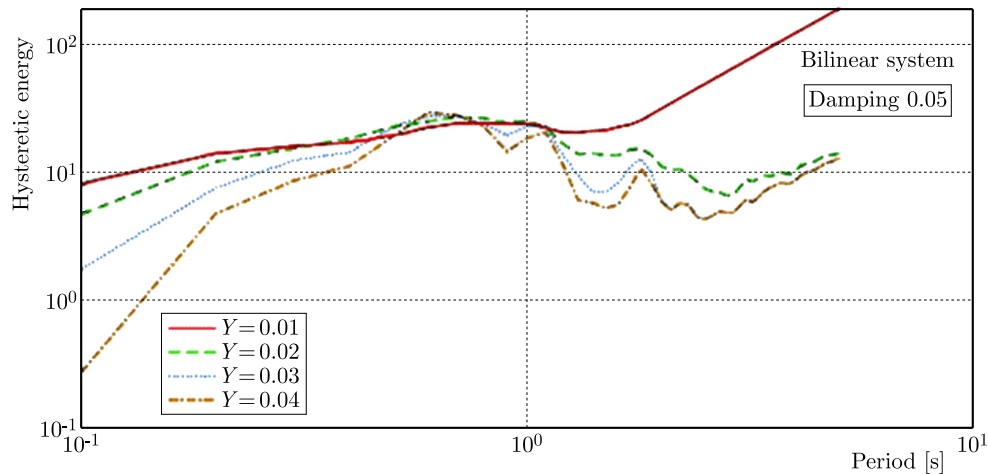

Fig. 9. Impact of the elasticity ratio on hysteretic energy in a bilinear system.

The results, shown in Figs. 7 and 8, reveal a consistent decrease in spectral values with longer periods and similar trends between systems with reduced and bilinear stiffness.

The yield coefficient has been recognized as one of the foremost factors in the structural analysis of nonlinear systems (Brahimi & Smain, 2021), because the initial yield displacement is a prerequisite for the inelastic reaction. Thus, Fig. 9 illustrates classical descriptions of mean displacement ductility for varying yield coefficients, assuming a system with bilinear stiffness and 5 % damping.

8. Conclusions

It has been demonstrated that by applying simulated ARMA processes within a time-domain approach, satisfactory results can be achieved with fewer parameters. The response spectra of simulated earthquakes closely resemble those of real earthquakes, except for long-period events. Studies have revealed a linear relationship between the logarithms of the mean nonlinear response spectrum and the system's natural period, indicating that an increase in the period results in a decrease in the average displacement ductility and hysteretic energy. Specifically, as the logarithm of the system's period increases, the response spectra for displacement, ductility, and hysteretic energy decrease for a given period and damping. The findings in this study, shown in time series form, converge with theoretical results and can be generalized. This could represent a significant advancement in the measurement and monitoring of stability in construction zones. We believe that these results can provide valuable insights for construction companies and society at large.

References

1. Ay, A.M. & Wang, Y. (2014). Structural damage identification based on self-fitting ARMAX model and multi-sensor data fusion. *Structural Health Monitoring*, *13*(4), 445–460. https://doi.org/10.1177/1475921714542891

2. Bodeux, J.B. & Golinval, J.C. (2001). Application of ARMAV models to the identification and damage detection of mechanical and civil engineering structures. *Smart Materials and Structures*, *10*(3), 479–489. https://doi.org/10.1088/0964-1726/10/3/309

3. Box, G.E., Jenkins, G.M., Reinsel, G.C., & Ljung, G.M. (2015). *Time series analysis: Forecasting and control*. John Wiley & Sons.

4. Brahimi, M. (1989). *The use of ARMA models for earthquake response spectra*. Polytechnic Institute of Brooklyn.

5. Brahimi, T. & Smain, T. (2021). A nonstationary mathematical model for acceleration time series. *Mathematical Modelling of Engineering Problems*, *8*(2), 246–252. https://doi.org/10.18280/mmep.080211

6. Carden, E.P. & Brownjohn, J.M. (2008). ARMA modelled time-series classification for structural health monitoring of civil infrastructure. *Mechanical Systems and Signal Processing*, *22*(2), 295–314. https://doi.org/10.1016/j.ymssp.2007.07.003

7. El-Choum, M.K. (2014). Utilization of ARMA models to measure damage potential in seismic records. In K. Chantawarangul (Ed.), *Sustainable Solutions in Structural Engineering and Construction* (pp. 138–143). Fargo, USA: ISEC Press. http://dx.doi.org/10.14455/ ISEC.res.2014.58

8. Johnson, E.A., Lam, H.F., Katafygiotis, L.S., & Beck, J.L. (2004). Phase I IASC-ASCE structural health monitoring benchmark problem using simulated data. *Journal of Engineering Mechanics*, *130*(1), 3–15. https://doi.org/10.1061/(ASCE)0733-9399(2004)130:1(3)

9. Luo, W.F. & Yu, L. (2017). New damage-sensitive feature for structures with bolted joints. *Journal of Physics: Conference Series*, *842*(1), Article 012083. IOP Publishing. https://doi.org/10.1088/1742-6596/842/1/012083

10. Menasri, A. (2012). *Simulation of strong motion with the ARMA technique* (in French). [Doctoral dissertation, Ecole Nationale Polytechnique].

11. Menasri, A., Brahimi, M., Frank, R., & Bali, A. (2012). ARMA modeling of artificial accelerograms for Algeria. *Applied Mechanics and Materials*, *105–107*, 348–355. https://doi.org/10.4028/www.scientific.net/AMM.105-107.348

12. Nair, K.K., Kiremidjian, A.S., & Law, K.H. (2006). Time series-based damage detection and localization algorithm with application to the ASCE benchmark structure. *Journal of Sound and Vibration*, *291*(1–2), 349–368. https://doi.org/10.1016/j.jsv.2005.06.016

13. Ouzandja, D., Messaad, M., Berrabah, A.T., & Belhrizi, M. (2023). Impact of material nonlinearity of dam-foundation rock system on seismic performance of concrete gravity dams. *Journal of Theoretical and Applied Mechanics*, *61*(1), 49–63. https://doi.org/10.15632/jtam-pl/157571

14. Sakellariou, J.S. & Fassois, S.D. (2006). Stochastic output error vibration-based damage detection and assessment in structures under earthquake excitation. *Journal of Sound and Vibration*, *297*(3–5), 1048–1067. https://doi.org/10.1016/j.jsv.2006.05.009

15. Zhang, Q.W. (2007). Statistical damage identification for bridges using ambient vibration data. *Computers & Structures*, *85*(7–8), 476–485. https://doi.org/10.1016/j.compstruc.2006.08.071

16. Zheng, H. & Mita, A. (2007). Two-stage damage diagnosis based on the distance between ARMA models and pre-whitening filters. *Smart Materials and Structures*, *16*(5), Article 1829. https://doi.org/10.1088/0964-1726/16/5/038